LINEAR MULTISTEP SOLVER DISTILLATION FOR FAST SAMPLING OF DIFFUSION MODELS

Anonymous authors
Paper under double-blind review

ABSTRACT

Sampling from diffusion models can be seen as solving the corresponding probability flow ordinary differential equation (ODE). The solving process requires a significant number of function evaluations (NFE), making it time-consuming. Recently, several solver search frameworks have attempted to find better-performing model-specific solvers. However, predicting the impact of intermediate solving strategies on final sample quality remains challenging, rendering the search process inefficient. In this paper, we propose a novel method for designing solving strategies. We first introduce a unified prediction formula for linear multistep solvers. Subsequently, we present a solver distillation framework, which enables a student solver to mimic the sampling trajectory generated by a teacher solver with more steps. We utilize the mean Euclidean distance between the student and teacher sampling trajectories as a metric, facilitating rapid adjustment and optimization of intermediate solving strategies. The design space of our framework encompasses multiple aspects, including prediction coefficients, time step schedules, and time scaling factors. Our framework has the ability to complete a solver search for Stable-Diffusion in less than 10 total GPU hours. Compared to previous reinforcement learning-based search frameworks, our approach achieves over a $10\times$ increase in search efficiency. With just 5 NFE, we achieve FID scores of 3.23 on CIFAR10, 7.16 on ImageNet-64, 5.44 on LSUN-Bedroom, and 15.69 on MS-COCO, resulting in a $2\times$ sampling acceleration ratio compared to handcrafted solvers.

1 INTRODUCTION

Diffusion models (Sohl-Dickstein et al., 2015; Ho et al., 2020; Song et al., 2021b) have gained widespread success in various applications including image generation (Dhariwal & Nichol, 2021; Rombach et al., 2022), audio synthesis (Kong et al., 2021; Chen et al., 2021), video generation (Ho et al., 2022b;a; Blattmann et al., 2023), and text-to-image synthesis (Saharia et al., 2022; Ruiz et al., 2023; Podell et al., 2024; Esser et al., 2024). When generating samples, diffusion models perform reverse solving of a predefined Stochastic Differential Equation (SDE) or its corresponding Probability Flow Ordinary Differential Equation (ODE) (Song et al., 2021b). This solving process often required hundreds of function evaluations (NFE), making it extremely time-consuming compared to classical generative models like Generative Adversarial Networks (GANs) (Goodfellow et al., 2014).

Fortunately, significant advancements have been made in accelerating the sampling process of diffusion models. Existing acceleration methods can be broadly categorized into two classes. The first class of methods involves an additional distillation training phase (Luhman & Luhman, 2021; Salimans & Ho, 2022; Song et al., 2023b; Sauer et al., 2023; Luo et al., 2024). Distilled models require only 1-4 NFE to generate high-quality samples. However, the distillation phase typically requires several GPU days, posing a significant training cost, especially for large scale models. Additionally, many of distilled models lack the ability to perform downstream tasks, such as image editing and restoration (Kawar et al., 2021; 2022; Meng et al., 2022; Song et al., 2022; 2023a; Chung et al., 2023). And the second class, which is also widely regarded, focuses on designing efficient solvers without further training the model. Techniques such as parameterization, exponential integrators, and higher-order solvers have successfully reduced the NFE to 15-20 for the sampling process (Lu et al., 2022b; Zhao et al., 2023; Zhang & Chen, 2022; Liu et al., 2022; Lu et al., 2022a; Song et al.,

Figure 1: Synthesized images of Stable-Diffusion (Rombach et al., 2022) with default classifier-free guidance scale 7.5 and text prompt *"A large **brown** bear walking through a forest"*. Our proposed DLMS can generate more realistic and visually detailed images compared with previous handcrafted samplers (Zhang & Chen, 2022; Lu et al., 2022b; Zhao et al., 2023).

2021a; Karras et al., 2022). However, when the NFE is less than 10, the sample quality deteriorates significantly.

The challenges have given rise to a series of search frameworks seeking more efficient solvers. However, due to the iterative nature of solving processes, it is difficult to predict the impact of intermediate solving strategies on the final sample quality, making the search process difficult and inefficient. These frameworks still often require tens of GPU hours and were limited to specific design space such as time steps (Watson et al., 2022; Li et al., 2023; Liu et al., 2023a; Sabour et al., 2024; Chen et al., 2024), parameterization mode (Zheng et al., 2023), or solver combination (Liu et al., 2023b).

In this paper, we propose a solver distillation framework that greatly accelerates the search efficiency. We begin by presenting a unified prediction formula for linear multistep solvers. Next, we introduce our solver distillation algorithm, which allows a student solver to replicate the sampling trajectory of a teacher solver that uses more steps. We employ the mean Euclidean distance between the student and teacher sampling trajectories as a metric, enabling quick adjustments and optimization of intermediate solving strategies. Compared to previous reinforcement learning-based search frameworks, our approach achieves over a $10\times$ increase in search efficiency.

Our framework has the ability to complete a solver distillation for Stable-Diffusion (Rombach et al., 2022) in less than 1.5h on 8 NVIDIA V100 GPUs. The design scope includes the time steps, the time scaling factors and the prediction coefficients. We extensively evaluate our approach on various resolution datasets in both pixel space and latent space. The *Distilled Linear Multistep Solver* (DLMS) significantly surpasses previous handcrafted and search-based solvers. Compared to handcrafted solvers, DLMS achieves a $2\times$ sampling acceleration ratio.

2 Background and Related Work

2.1 Diffusion Models

Given the data distribution p_0, diffusion models employ a *forward process* $\mathbf{x}_t = \alpha_t \mathbf{x}_0 + \sigma_t \epsilon, t \in [0, T]$ with marginal distribution $\{p_t\}_0^T$ to gradually degenerate the data $\mathbf{x}_0 \sim p_0$ with Gaussian

noise $\epsilon \sim \mathcal{N}(\mathbf{0}, \boldsymbol{I})$. The *noise schedule* $\alpha_t, \sigma_t > 0$ is designed to make p_T approximately a pure Gaussian distribution $\mathcal{N}(\mathbf{0}, \tilde{\sigma}^2 \boldsymbol{I})$. Notably, there exists a corresponding *Probability Flow* ordinary differential equation (PF-ODE) (Song et al., 2021b):

$$\mathrm{d}\mathbf{x}_t = \left[f(t)\mathbf{x}_t - \frac{1}{2} g^2(t) \nabla \log p_t(\mathbf{x}_t) \right] \mathrm{d}t, \tag{1}$$

where $f(t) = \frac{\mathrm{d}\log \alpha_t}{\mathrm{d}t}, g^2(t) = \frac{\mathrm{d}\sigma_t^2}{\mathrm{d}t} - 2\frac{\mathrm{d}\log \alpha_t}{\mathrm{d}t}\sigma_t^2$(Kingma et al., 2021). The PF-ODE shares the same marginal distribution p_t as the forward process. And the score function $\nabla \log p_t(\mathbf{x}_t)$ can be expressed using Tweedie's formula (Robbins, 1992):

$$\nabla \log p_t(\mathbf{x}_t) = \frac{\alpha_t \mathbb{E}[\mathbf{x}_0|\mathbf{x}_t] - \mathbf{x}_t}{\sigma_t^2} = -\frac{\mathbb{E}[\epsilon|\mathbf{x}_t]}{\sigma_t}. \tag{2}$$

To estimate the score function, a neural network $\epsilon_\theta(\mathbf{x}_t, t)$ is trained to predict $\mathbb{E}[\epsilon|\mathbf{x}_t]$ via the least square estimation by minizing the L_2 loss

$$\mathbb{E}_{\mathbf{x}_0 \sim p_{\mathrm{data}}, \epsilon \sim \mathcal{N}(\mathbf{0}, \boldsymbol{I})} \left\| \epsilon_\theta(\mathbf{x}_t, t) - \epsilon \right\|_2^2 \tag{3}$$

for each $t \in [0, T]$. Consequently, we can sample from diffusion models by solving the empirical PF-ODE:

$$\mathrm{d}\mathbf{x}_t = \left[f(t)\mathbf{x}_t + \frac{g^2(t)}{2\sigma_t} \epsilon_\theta(\mathbf{x}_t, t) \right] \mathrm{d}t \tag{4}$$

from time T to time 0. Additionally, the conditional sampling can be carry out by guided sampling (Dhariwal & Nichol, 2021; Ho & Salimans, 2021). Remarkably, classifier-free guidance (Ho & Salimans, 2021) defines a guided noise predictor:

$$\tilde{\epsilon}_\theta(\mathbf{x}_t, t, c) = s \cdot \epsilon_\theta(\mathbf{x}_t, t, c) + (1 - s) \cdot \epsilon_\theta(\mathbf{x}_t, t, \emptyset), \tag{5}$$

where c is the condition, $\emptyset$ stand for the unconditional sampling, and $s > 0$ is the guidance scale.

In practice, except for the noise predictor $\epsilon_\theta(\mathbf{x}_t, t)$, diffusion models can also be parameterized as data predictor $\boldsymbol{x}_\theta(\mathbf{x}_t, t)$ to predict $\mathbf{x}_0$ or velocity predictor $\boldsymbol{v}_\theta(\mathbf{x}_t, t)$ to predict $\alpha_t \epsilon - \sigma_t \mathbf{x}_0$, where the parameterizations are theoretically equivalent, but have impact in practice performance(Karras et al., 2022; Hang et al., 2023).

2.2 Fast sampling with Exponential Integrators

Samplers based on exponential integrator have been found to be more efficient than directly solving the ODE (4). Given an initial value $\mathbf{x}_s$ at time s, the ODE solution $\mathbf{x}_t$ can be analytically computed with the following exponentially weighted integral by changing the variable from t to half log-SNR $\lambda_t := \log(\alpha_t / \sigma_t)$ (Lu et al., 2022a;b):

$$\mathbf{x}_t = \frac{\alpha_t}{\alpha_s}\mathbf{x}_s - \alpha_t \int_{\lambda_s}^{\lambda_t} e^{\lambda} \hat{\epsilon}_\theta(\hat{\mathbf{x}}_\lambda, \lambda) \mathrm{d}\lambda, \mathbf{x}_t = \frac{\sigma_t}{\sigma_s}\mathbf{x}_s + \sigma_t \int_{\lambda_s}^{\lambda_t} e^{-\lambda} \hat{\boldsymbol{x}}_\theta(\hat{\mathbf{x}}_\lambda, \lambda) \mathrm{d}\lambda \tag{6}$$

where $\hat{\epsilon}_\theta(\cdot, \lambda) := \epsilon_\theta(\cdot, t(\lambda)), \hat{\mathbf{x}}_\theta(\cdot, \lambda) := \boldsymbol{x}_\theta(\cdot, t(\lambda))$ and $\hat{\mathbf{x}}_\lambda := \mathbf{x}_{t(\lambda)}$. To predict the integral part, DEIS (Zhang & Chen, 2022) approximates $\epsilon_\theta(\mathbf{x}_t, t)$ with polynomial interpolation w.r.t t , similarly DPM-Solver (Lu et al., 2022a) approximate $\hat{\epsilon}_\theta(\hat{\mathbf{x}}_\lambda, \lambda)$ w.r.t λ (equation 6, left) and DPM-Solver++ (Lu et al., 2022b) approximate $\hat{\boldsymbol{x}}_\theta(\hat{\mathbf{x}}_\lambda, \lambda)$ w.r.t λ (equation 6, right). UniPC (Zhao et al., 2023) introduces a correcting strategy and various scale functions. And AMED-Solver (Zhou et al., 2024) adopts an approximate mean value method instead polynomial interpolation.

2.3 Efficient Sampler Search

Recently, several frameworks have incorporated a search phase to enhance the efficiency of samplers. The time step schedule is a commonly explored aspect (Chen et al., 2024; Sabour et al., 2024; Li et al., 2023; Watson et al., 2022; Liu et al., 2023a). Moreover, DPM-Solver-v3 (Zheng et al., 2023) aims to optimize the parameterization mode beyond noise prediction and data prediction. USF (Liu et al., 2023b) strives to identify the most suitable solver for each time step.

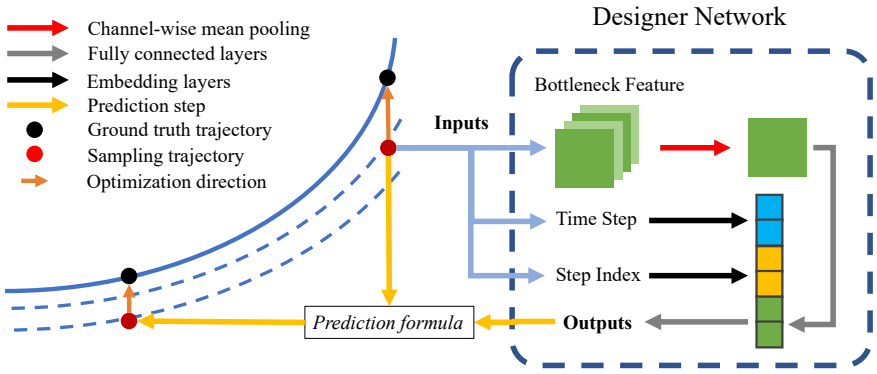

Figure 2: Designer network architecture. We concatenate the embeddings of the bottleneck feature, time step, and step index, and pass them through a fully connected layer to obtain the parameters required for the *prediction formula* (7, 8).

3 METHODOLOGY

In this section, we present our method to solve the PF-ODE (4). We start with the discussion about the optimal linear multistep prediction strategy. And then we introduce how to achieve the optimal solver with an adaptive time schedule and time scaling factors. Finally, we introduce some practical techniques to further improve performance.

3.1 TOWARDS OPTIMAL LINEAR MULTISTEP SOLVER

Given a time schedule $\{t_n\}_{n=0}^N$ decreasing from $t_0 = T$ to $t_N = 0$, the solvers are trying to predict the ground truth trajectory $\{\mathbf{x}_{t_n}^G\}_{n=0}^N$ with a numerical simulation trajectory $\{\mathbf{x}_{t_n}^S\}_{n=0}^N$ with $\mathbf{x}_{t_0}^S = \mathbf{x}_{t_0}^G$. Linear multistep solvers aim to predict each local intermediate $\mathbf{x}_{t_n}^G, n \geq 1$ by leveraging the linear combination of p precious outputs from the denoising network. Take the data prediction type (equation 6, right) for example, the *prediction formula* can be expressed as:

$$\boldsymbol{D}_n = \sum_{k=1}^{p} a_k \boldsymbol{x}_\theta(\mathbf{x}_{t_{n-k}}^S, s_{n-k} t_{n-k}), \tag{7}$$

$$\mathbf{x}_{t_n}^S = \frac{\sigma_{t_n}}{\sigma_{t_{n-1}}} \mathbf{x}_{t_{n-1}}^S - \alpha_{t_n}(e^{\lambda_{t_{n-1}} - \lambda_{t_n}} - 1)\boldsymbol{D}_n \tag{8}$$

where $\{a_k\}_{k=1}^p$ are the prediction coefficients and the time scaling factors $\{s_n\}_{n=0}^N$ are usually set to 1. This implies that the candidate $\mathbf{x}_{t_n}^S$ lies in a p-dimensional hyperplane and hence the theoretically optimal $\mathbf{x}_{t_n}^S$ is the linear projection of $\mathbf{x}_{t_n}^G$ onto the hyperplane.

It is worth noting that for each trajectory $\{\mathbf{x}_{t_n}^G\}_{n=0}^N$ and for each step n the optimal coefficients $\{a_k^*\}_{k=1}^p$ are different. Nevertheless, some studies have shown that the ODE trajectories from diffusive models have similar properties(Chen et al., 2024), so it is possible to design a unified $\{a_k\}_{k=1}^p$ that works well on all trajectories just as in most of previous works, but we consider this to be a suboptimal choice.

As mentioned in the previous paragraph, we aim to assign distinct coefficients for each trajectory and step. To achieve this, we establish a mapping $g : (\mathbf{x}_{t_{n-1}}^S, t_{n-1}, n-1) \longmapsto \{a_k\}_{k=1}^p$. Drawing inspiration from Zhou et al. (2024) we utilize the bottleneck feature $\boldsymbol{h}_{t_{n-1}}$ obtained from the pretrained denoising model instead of $\mathbf{x}_{t_{n-1}}^S$ to circumvent additional computational costs. Subsequently, we employ an extremely lightweight *designer network* $g_\phi(\boldsymbol{h}_{t_{n-1}}, t_{n-1}, n-1)$ to generate the coefficients $\{a_k\}_{k=1}^p$. The network architecture is shown in Fig. 2. Given the availability of the ground truth trajectory $\{\mathbf{x}_{t_n}^G\}_{n=0}^N$, we can establish the optimal solver by minimizing the square distance $d(\mathbf{x}_{t_n}^S, \mathbf{x}_{t_n}^G)$ where the prediction $\mathbf{x}_{t_n}^S$ is computed using equations (7) and (8) with $\{a_k\}_{k=1}^p = g_\phi(\boldsymbol{h}_{t_{n-1}}, t_{n-1}, n-1)$. In practical terms, we utilize a numerical ground truth trajectory $\mathbf{x}_{t_n}^T$ generated by a teacher solver Φ_t such as DPM-Solver++ with M interpolation time steps between t_{n-1} and t_n, which we denote as $\mathbf{x}_{t_n}^T = \Phi_t(\mathbf{x}_{t_{n-1}}^T, t_{n-1}, t_n, M)$.

3.2 ADAPTIVE TIME SCHEDULE

Adaptive time schedule is a class of approaches that can significantly improve the efficiency of various solvers. Some previous works (Xia et al., 2024; Zhou et al., 2024) also show that adjusting the time scaling factors $\{s_n\}_{k=1}^N$ properly can improve the accuracy of the solution. In Sec. 3.1, we described how to get the distilled solver for a fixed time schedule $\{t_n\}_{n=0}^N$. In this section, we show how to use our distillation framework to get adaptive time schedules.

When adjusting the prediction coefficients $\{a_k\}_{k=1}^p$ in Sec. 3.1, we chose $\mathbf{x}_{t_{n-1}}^S$ at time t_{n-1} as the starting point to predict $\mathbf{x}_{t_n}^G$. Now, we aim to incorporate t_{n-1} and s_{n-1} into the design space. Therefore, we modify the starting point to be $\mathbf{x}_{t_{n-2}}^S$ at time t_{n-2}. To ensure each trajectory has an independent adaptive time schedule rather than a unified schedule, we include the time schedules $\{t_n\}_{n=0}^N$ and $\{s_n\}_{n=0}^N$ in the output of g_ϕ. This is achieved by setting $\{a_k\}_{k=1}^p, t_{n-1}, s_{n-1} = g_\phi(\boldsymbol{h}_{t_{n-2}}, t_{n-2}, n-2)$ for $n \geq 2$. Let Q denote the buffer list that collects outputs $\boldsymbol{x}_\theta(\mathbf{x}_{t_n}^S, s_n t_n)$. We write the *prediction formula* (7, 8) as:

$$\mathbf{x}_n^S = \Phi(\mathbf{x}_{n-1}^S, t_{n-1}, t_n, \{a_k\}_{k=1}^p, Q). \tag{9}$$

Thus, the distillation phase can be summarized by Algorithm 1. After the distillation phase, Algorithm 2 shows the sampling process with a trained designer network g_ϕ. It is worth noting that we

Algorithm 1 Linear Multistep Solver Distillation

Require: Designer network g_ϕ, teacher solver Φ_t, number of time steps N, number of interpolation time steps M, initial timestep T, max order p.

repeat
  Sample initial value $\mathbf{x}_{t_0}^S = \mathbf{x}_{t_0}^T \sim \mathcal{N}(\mathbf{0}, \tilde{\sigma}^2 \boldsymbol{I})$
  $t_0 \leftarrow T, s_0 \leftarrow 1$. Initialize an empty buffer Q.
  Set the parameter gradient of ϕ to 0
  $Q \xleftarrow{\text{buffer}} \boldsymbol{x}_\theta(\mathbf{x}_{t_0}^S, s_0 t_0)$
  Extract the bottleneck feature h_{t_0}
  for $n = 2$ to N **do**
    $\{a_k\}_{k=1}^{\max(n-1,p)}, t_{n-1}, s_{n-1} \leftarrow g_\phi(\boldsymbol{h}_{t_{n-2}}, t_{n-2}, n-2)$
    $\mathbf{x}_{t_{n-1}}^S \leftarrow \Phi(\mathbf{x}_{n-2}^S, t_{n-2}, t_{n-1}, \{a_k\}_{k=1}^{\max(n-1,p)}, Q)$ ▷ Generate prediction $\mathbf{x}_{t_{n-1}}^S$.
    $Q \xleftarrow{\text{buffer}} \boldsymbol{x}_\theta(\mathbf{x}_{t_{n-1}}^S, s_{n-1} t_{n-1})$
    Extract the bottleneck feature $h_{t_{n-1}}$
    $\{a_k\}_{k=1}^{\max(n,p)}, t_n, s_n \leftarrow g_\phi(\boldsymbol{h}_{t_{n-1}}, t_{n-1}, n-1)$
    $t_n \leftarrow \mathrm{sg}(\mathrm{t_n})$ ▷ Stop the gradient of t_n.
    $\mathbf{x}_{t_n}^S \leftarrow \Phi(\mathbf{x}_{n-1}^S, t_{n-1}, t_n, \{a_k\}_{k=1}^{\max(n,p)}, Q)$ ▷ Generate prediction $\mathbf{x}_{t_n}^S$.
    if n=2 **then**
      $\mathbf{x}_{t_{n-1}}^T \leftarrow \mathrm{sg}(\Phi_\mathrm{t}(\mathbf{x}_{\mathrm{t}_{n-2}}^\mathrm{T}, \mathrm{t}_{n-2}, \mathrm{t}_{n-1}, \mathrm{M}))$
    end if
    $\mathbf{x}_{t_n}^T \leftarrow \mathrm{sg}(\Phi_\mathrm{t}(\mathbf{x}_{\mathrm{t}_{n-1}}^\mathrm{T}, \mathrm{t}_{n-1}, \mathrm{t}_n, \mathrm{M}))$ ▷ Solve the numerical ground truth $\mathbf{x}_{t_n}^T$.
    $\mathcal{L}_n(\phi) \leftarrow d(\mathbf{x}_{t_n}^S, \mathbf{x}_{t_n}^T)$ ▷ Calculate the prediction error at time t_n.
    Perform backpropagation for $\mathcal{L}_n(\phi)$.
    $Q \leftarrow \mathrm{sg}(\mathrm{Q}), \mathrm{t}_{n-1} \leftarrow \mathrm{sg}(\mathrm{t}_{n-1})$ ▷ Stop the gradient of buffers and t_{n-1}
  end for
  Update the parameter ϕ
until convergence

have employed the stop gradient operation multiple times in Algorithm 1, which is crucial for the proper functioning of the algorithm. When using the state $\mathbf{x}_{t_{n-2}}^S$ at time t_{n-2} to predict $\mathbf{x}_{t_n}^T$ at time t_n, retaining the gradients of $t_{n-2}, t_n, \mathbf{x}_{t_{n-2}}^S, \mathbf{x}_{t_n}^T$ will lead to two issues:

- Firstly, the gradients from past time steps will not be removed from the computation graph, resulting in a linear increase in memory usage with each step n.
- Secondly, t_n will move towards t_{n-2} to ease the prediction difficulty, ultimately resulting in the collapse of the entire time schedule. This is not an ideal outcome.

Algorithm 2 Distilled Solver Sampling

Require: Designer network g_ϕ, number of time steps N, initial timestep T, max order p.
1: Sample initial value $\mathbf{x}_{t_0}^S \sim \mathcal{N}(\mathbf{0}, \tilde{\sigma}^2 \boldsymbol{I})$
2: $t_0 \leftarrow T, s_0 \leftarrow 1$. Initialize an empty buffer Q.
3: **for** $n = 1$ to N **do**
4: $\quad Q \xleftarrow{\text{buffer}} \boldsymbol{x}_\theta(\mathbf{x}_{t_{n-1}}^S, s_{n-1}t_{n-1})$
5: $\quad$ Extract the bottleneck feature $h_{t_{n-1}}$
6: $\quad \{a_k\}_{k=1}^{\max(n,p)}, t_n, s_n \leftarrow g_\phi(\boldsymbol{h}_{t_{n-1}}, t_{n-1}, n-1)$
7: $\quad \mathbf{x}_{t_n}^S \leftarrow \Phi(\mathbf{x}_{n-1}^S, t_{n-1}, t_n, \{a_k\}_{k=1}^{\max(n,p)}, Q)$
8: **end for**
9: **return** $\mathbf{x}_{t_N}^S$

In addition, we find it necessary to adopt data prediction type (equation 6, right). We believe this is because the data prediction type can automatically align the noise intensity with the time step t to stabilize the prediction error of the solver.

3.3 Practical Techniques

In this section, we introduce several practical techniques to further improve the performance of DLMS.

High-order initialization. Since the prediction formula (7, 8) covers almost all linear multi-step solvers with exponential integrators such as DDIM (Song et al., 2021a), PLMS(iPNDM) (Zhang & Chen, 2022; Liu et al., 2022), DPM-Solver++ (Lu et al., 2022b), UniP-p (Zhao et al., 2023) and DEIS (Zhang & Chen, 2022). We can initialize with these pre-designed solvers by setting the output biases of the designer network g_ϕ. Therefore, DLMS has a theoretical accuracy that is at least on par with the aforementioned methods. Thus, we still refer to the number of history outputs p used in each step as the "order". Although our framework still works with DDIM (Song et al., 2021a) initialization, using higher-order solvers allows the distillation phase to be completed more quickly with fewer generated trajectories. In our experiments, initializing with any higher-order methods did not show significant differences; for simplicity, we recommend PLMS (Zhang & Chen, 2022; Liu et al., 2022) as the initial solving strategy. Its prediction coefficients are as follows:

$$p = 1, a_1 = 1 \tag{10}$$

$$p = 2, (a_1, a_2) = (\frac{3}{2}, -\frac{1}{2}) \tag{11}$$

$$p = 3, (a_1, a_2, a_3) = (\frac{23}{12}, -\frac{16}{12}, \frac{5}{12}) \tag{12}$$

$$p = 4, (a_1, a_2, a_3, a_4) = (\frac{55}{24}, -\frac{59}{24}, \frac{37}{24}, -\frac{9}{24}) \tag{13}$$

Analytical First Step (AFS). In Algorithm 1, the initial time step $t_0 = T$ and time scaling factor $s_0 = 1$ are excluded from the design space. Instead, we can treat $t_0 = T$ as a virtual initial step. Specifically, we set $\boldsymbol{x}_\theta(\mathbf{x}_{t_0}^S, s_0 t_0) = \mathbf{0}$ and $h_{t_0} = \mathbf{0}$, without employing the denoising network. This approach ensures that t_1 is the actual first time step at which the diffusion model is engaged, while t_1 and s_1 remain in the design space. This strategy is fundamentally equivalent to the *analytical first step* (AFS) proposed by Dockhorn et al. (2022).

Exponential Moving Average (EMA). Due to NFE limitations, the student solver cannot fully replicate the sampling trajectory generated by the teacher solver. This leads to a non-zero stochastic gradient even at convergence. To reduce the impact of parameter oscillations on solver performance, we introduce EMA updates inspired by diffusion models. During solver distillation, we apply EMA updates with half-lives of 1, 2, and 3 kimg, selecting the best-performing configuration from four parameter sets.

Inception distance at the final step. Some search-based frameworks directly use Fréchet Inception Distance (FID) (Heusel et al., 2017) as the optimization objective (Liu et al., 2023b; Watson et al., 2022; Li et al., 2023). In contrast, our method employs square distance as the optimization target.

Since square distance is less sensitive to high-frequency information, we observe that optimizing square distance does not always lead to better FID scores. Therefore, in experiments conducted in pixel space, we replace the final step's objective from pixel square distance to Inception Distance (the square distance of features from the Inception network). We only make this replacement in the final step because we find that Inception Distance does not effectively capture the differences between noisy images. In latent space tasks, the issue of high-frequency information is not present. To avoid unnecessary calls to the network modules, we do not perform this replacement in those cases.

3.4 Comparing with Related Methods

Comparing with Progressive Distillation. Progressive distillation (Salimans & Ho, 2022) is a distillation method for diffusion models that gradually distills the results of multi-step solvers into fewer steps. In our framework, we also employ a multi-step teacher solver and aim to distill the results into our student solver with fewer steps. However, our approach does not require training the parameters of the diffusion model, while the parameter requirements and training duration for progressive distillation (PD) are thousands of times greater than those of our framework.

Comparing with AMED-Plugin. AMED-Plugin(Zhou et al., 2024) is a method for selecting intermediate time steps for existing solvers and time schedules. The designer network g_ϕ used in our work is modified from AMED-Plugin. In contrast, the DLMS in this paper do not rely on existing solvers or time schedules. AMED-Plugin can be seen as adjusting half of the time schedule, while our proposed adaptive time schedule method is for full time schedule adjustment.

Comparing with USF. USF (Liu et al., 2023b) is a search framework based on reinforcement learning. The authors train a predictor network to estimate the FID performance of a solver with specific hyperparameters, using this to guide an evolutionary search process for hyperparameter optimization. The relationship between hyperparameters and performance is complex, making the training of a predictor network both challenging and time-consuming.

In contrast, our framework leverages local prediction error to design an optimal solution strategy, which aligns more closely with the iterative nature of the sampling process and the criteria for manually designing solvers. Furthermore, while USF simply combines existing handcrafted solvers, our approach utilizes prediction formulas (7, 8) to achieve a true unification of multiple solving strategies. This enables us to develop new solving strategies by learning the prediction coefficients $\{a_k\}_{k=1}^{p}$.

4 Experiments

In this section, we demonstrate that DLMS exhibits significant advantages in both unconditional and conditional sampling with pixel-space and latent-space diffusion models. We conducted experiments across multiple datasets with resolutions ranging from 32 to 512 and compared our approach with current state-of-the-art both handcrafted and search-based solvers. Then, we showcase the benefits across various aspects of the design space, as well as the ablation studies of the practical techniques we provided. Finally, we visualize the adaptive time schedules and the samples generated by DLMS.

5 Datasets and Settings

In our experiments, we uniformly use the noise schedule $\alpha_t = 1, \sigma_t = t$ from Karras et al. (2022). We initialized the prediction coefficients with PLMS (Zhang & Chen, 2022; Liu et al., 2022), using a uniform time schedule (Ho et al., 2020) and time scaling factors of 1. We use DPM-Solver++ (Lu et al., 2022b) to generate ground truth trajectories. The designer network g_ϕ consists of a two-layer MLP with a total parameter count of only 9k. We use Adam as the optimizer with a learning rate of 5×10^{-3}. To ensure fairness, we use the same random seed to evaluate the FID score.

EDM on CIFAR10, FFHQ, ImageNet-64. The sampling on CIFAR10 (Krizhevsky et al., 2009) 32×32 , FFHQ (Karras et al., 2019) 64×64, ImageNet-64 (Deng et al., 2009) 64×64 is based on the pretrained pixel-space diffusion model provided by EDM (Karras et al., 2022). Among these, ImageNet-64 is for conditional sampling and CIFAR10, FFHQ are for unconditional Sampling. The

order p for student solver DLMS is set to 4. The number of interpolation time steps M is set to 4. For each dataset, we conduct solver distillation on 20k trajectories. The distillation times are approximately 5 min, 10 min, and 17 min, respectively, on 8 NVIDIA V100 GPUs. We measure sample quality using the FID score calculated on 50k generated images.

Latent-Diffusion on LSUN-Bedroom. The unconditional sampling on LSUN-Bedroom (Yu et al., 2015) 256×256, is based on the pretrained latent-space diffusion model provided by Latent-Diffusion (Rombach et al., 2022). The order p for student solver DLMS is set to 3. The number of interpolation time steps M is set to 1. We conduct solver distillation on 10k trajectories. The distillation times are approximately 20min on 8 NVIDIA V100 GPUs. We measure sample quality using the FID score calculated on 50k generated images.

Guided-Diffusion on ImageNet. The conditional sampling on ImageNet (Deng et al., 2009) 256×256, is based on the pretrained pixel-space diffusion model provided by Guided-Diffusion (Dhariwal & Nichol, 2021). The order p for student solver DLMS is set to 3. The number of interpolation time steps M is set to 3. We conduct solver distillation on 5k trajectories with default guidance scale 2.0. The distillation times are approximately 40min on 8 NVIDIA V100 GPUs. We measure sample quality using the FID score calculated on 10k generated images.

Stable-Diffusion on MS-COCO prompts. The text-to-image sampling on MS-COCO(2014) (Lin et al., 2014) 512×512, is based on the pretrained latent-space diffusion model provided by Stable-Diffusion v1.5 (Rombach et al., 2022). The order p for student solver DLMS is set to 2. The number of interpolation time steps M is set to 1. We conduct solver distillation on 5k trajectories with default guidance scale 7.5. The distillation times are approximately 1.5h on 8 NVIDIA V100 GPUs. We measure sample quality using the FID score calculated on 30k generated images generated by 30k prompts from the MS-COCO validation set.

5.1 Main Results

We select the current state-of-the-art artificially designed solvers as baseline methods, including DEIS Zhang & Chen (2022), DPM-Solver++ (Lu et al., 2022b), and UniPC (Zhao et al., 2023). All results are obtained from an open-source toolbox[1], utilizing the recommended settings from the original papers. Detailed results can be found in the Appendix A.

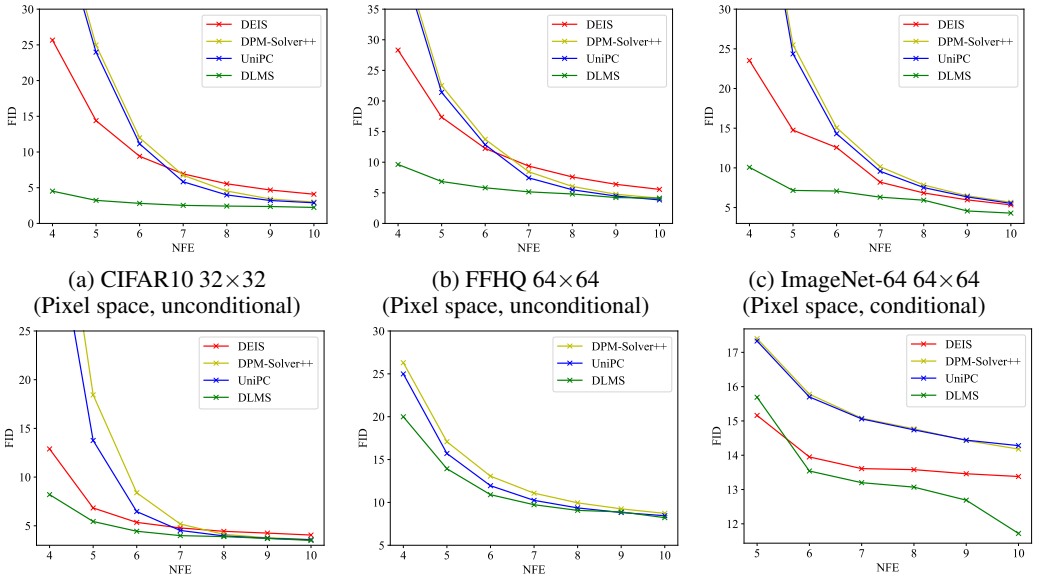

(a) CIFAR10 32×32 (Pixel space, unconditional)
(b) FFHQ 64×64 (Pixel space, unconditional)
(c) ImageNet-64 64×64 (Pixel space, conditional)
(d) LSUN-Bedroom 256×256 (Latent space, unconditional)
(e) ImageNet 256×256 (Pixel space, guidance scale 2.0)
(f) MS-COCO 512×512 (Latent space, guidance scale 7.5)

Figure 3: Comparison of FID↓ scores between DLMS and handcrafted solvers.

[1] https://github.com/zju-pi/diff-sampler.

Fig. 3 presents a comparison of FID scores between DLMS and previous handcrafted methods. As shown in Fig. 3, handcrafted solvers based on polynomial interpolation exhibit a sharp decline in performance as NFE decreases. In contrast, our proposed DLMS maintains high-quality sampling, demonstrating a significant advantage over baseline methods. In text-to-image generation with Stable-Diffusion (Rombach et al., 2022), DLMS achieves an FID of 13.54 with only 6 NFE, while the baseline methods require 10 NFE for comparable performance, resulting in a 2× acceleration ratio.

We further compare our method with other search frameworks. The methods include in the comparison are the reinforcement learning-based framework USF (Liu et al., 2023b), the parameterization-focused DPM-Solver-v3 (Zheng et al., 2023). Additionally, we include GITS (Chen et al., 2024), an outstanding adaptive time scheduling method, and AMED-Plugin (Zhou et al., 2024), a closely related work. As shown in Tab. 1, DLMS still stands out among various search frameworks.

Table 1: Comparison of FID↓ on CIFAR10 between DLMS and search-based solvers.

Solver	**NFE**						
	4	5	6	7	8	9	10
DPM-Solver-v3	-	12.21	8.56	-	3.50	-	2.51
USF	11.50	6.86	5.18	3.81	3.41	3.02	2.69
AMED-Plugin	-	6.61	-	3.65	-	2.63	-
GITS	10.11	6.77	4.29	3.43	2.70	2.42	2.28
DLMS	**4.52**	**3.23**	**2.81**	**2.53**	**2.43**	**2.37**	**2.24**

In Tab. 2, we compare the total GPU hours required for a 7 NFE solver with USF and DPM-Solver-v3. Due to limitations in code availability, the reported time costs are sourced from original papers and measured on different devices. Nevertheless, our method demonstrates a significant order-of-magnitude advantage, achieving a 10× increase in search efficiency.

Table 2: Comparison of total GPU hours for search phase.

Solver	**CIFAR10**	**MS-COCO**	**Device**
DPM-Solver-v3	28	88	NVIDIA A40
USF	12.15	106.64	NVIDIA 3090/A100
DLMS	**0.7**	**10**	NVIDIA V100

5.2 Ablation Study

Tab. 3 demonstrates the ablation effects of each component in the DLMS framework. As shown in the results, the time step-related time schedule and time scaling contribute the most significant improvements.

Table 3: FID results of ablation study on CIFAR10.

NFE	4	6	8	10
DLMS	**4.52**	**2.81**	2.43	**2.24**
w/o AFS	6.48	3.30	**2.42**	2.30
w/o bottleneck feature	4.71	3.40	2.46	2.25
w/o high-order initialization	4.92	3.25	2.94	2.44
w/o Inception distance	6.67	3.77	3.10	2.80
w/o time scaling	7.75	3.86	3.07	2.41
w/o adaptive time schedule	10.41	6.18	3.17	3.03
Handcrafted(best)	25.66	9.40	3.99	2.89

5.3 VISUALIZATIONS

Visual Quality. We present qualitative comparisons in Fig. 1. Handcrafted solvers struggle to generate vegetation and accurately colored bears with 5 NFEs. In contrast, DLMS effectively learns the generation results of the teacher solver with double NFEs. With 10 NFEs, DLMS is the only method that successfully produces the correct lighting and head pose. Additional samples are provided in Appendix B.

Visualization of adaptive time schedule. Fig. 4 shows the adaptive time schedules obtained from DLMS with 10 NFE using AFS. By comparing these schedules with handcrafted time schedules such as logSNR (Zheng et al., 2023; Lu et al., 2022b), polynomial (Karras et al., 2022), time uniform (Ho et al., 2020) and time square (Zhang & Chen, 2022), we uncover some intriguing findings. The adaptive time schedules exhibit striking differences across various datasets. For the CIFAR10 and FFHQ datasets, the adaptive time schedules are similar to the time square schedule. In contrast, for ImageNet-64 and LSUN-Bedroom, they resemble the time uniform schedule. Notably, the schedule learned for the Stable-Diffusion model aligns closely with the uniform logSNR schedule, except for the final step.

The observed differences may arise from several factors, including the solving strategy, image resolution, solving space, and guidance. For instance, in the EDM context, DPM-Solver++ (Lu et al., 2022b) and UniPC (Zhao et al., 2023) perform better with logSNR, while DEIS (Zhang & Chen, 2022) demonstrates superior performance with the time square schedule. However, on other models, all three solvers tend to prefer the time uniform schedule. This highlights the importance of simultaneously searching for both time schedules and solving strategies within our framework across different datasets.

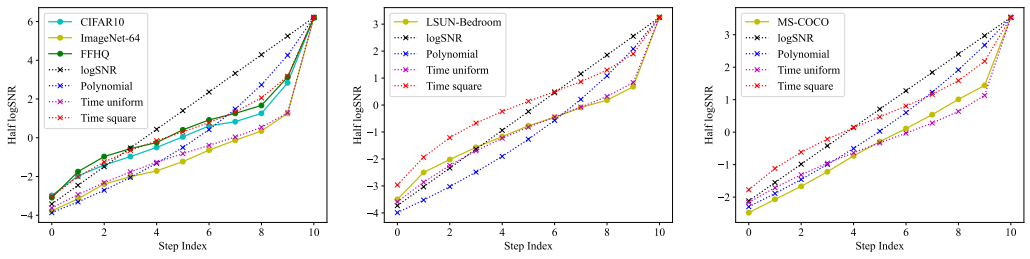

(a) EDM (b) Latent-Diffusion (c) Stable-Diffusion

Figure 4: Visualization of adaptive time schedule.

6 CONCLUSION

We propose a linear multistep solver distillation framework. Our framework enables the student solver to replicate the sampling trajectory of a teacher solver that utilizes more steps, facilitating rapid adjustments and optimization of prediction coefficients, time step schedules, and time scaling factors. Experiments demonstrate the effectiveness of our framework across various resolution datasets, using both pixel-space and latent-space pre-trained diffusion models, and reveal a significant improvement in sample quality with 4 10 NFEs.

Limitations and Future Work. Our framework is currently limited to ODE solvers, while in practice, stochastic samplers (Xue et al., 2024) often outperform deterministic samplers. Therefore, extending our method to stochastic samplers is a promising direction. Additionally, integrating our work with approaches such as Deepcache (Ma et al., 2024) and FreeU (Si et al., 2024) is also worth exploring.

REFERENCES

Andreas Blattmann, Robin Rombach, Huan Ling, Tim Dockhorn, Seung Wook Kim, Sanja Fidler, and Karsten Kreis. Align your latents: High-resolution video synthesis with latent diffusion models. In *Proceedings of the IEEE/CVF Conference on Computer Vision and Pattern Recognition*, pp. 22563–22575, 2023.

Defang Chen, Zhenyu Zhou, Can Wang, Chunhua Shen, and Siwei Lyu. On the trajectory regularity of ODE-based diffusion sampling. In *Forty-first International Conference on Machine Learning*, 2024.

Nanxin Chen, Yu Zhang, Heiga Zen, Ron J. Weiss, Mohammad Norouzi, and William Chan. Wavegrad: Estimating gradients for waveform generation. In *International Conference on Learning Representations*, 2021.

Hyungjin Chung, Jeongsol Kim, Michael Thompson Mccann, Marc Louis Klasky, and Jong Chul Ye. Diffusion posterior sampling for general noisy inverse problems. In *The Eleventh International Conference on Learning Representations*, 2023.

Jia Deng, Wei Dong, Richard Socher, Li-Jia Li, Kai Li, and Li Fei-Fei. Imagenet: A large-scale hierarchical image database. In *CVPR*, pp. 248–255. IEEE, 2009.

Prafulla Dhariwal and Alexander Quinn Nichol. Diffusion models beat GANs on image synthesis. In *Advances in Neural Information Processing Systems*, volume 34, pp. 8780–8794, 2021.

Tim Dockhorn, Arash Vahdat, and Karsten Kreis. Genie: Higher-order denoising diffusion solvers. *Advances in Neural Information Processing Systems*, 35:30150–30166, 2022.

Patrick Esser, Sumith Kulal, Andreas Blattmann, Rahim Entezari, Jonas Müller, Harry Saini, Yam Levi, Dominik Lorenz, Axel Sauer, Frederic Boesel, et al. Scaling rectified flow transformers for high-resolution image synthesis. *arXiv preprint arXiv:2403.03206*, 2024.

Ian J. Goodfellow, Jean Pouget-Abadie, Mehdi Mirza, Bing Xu, David Warde-Farley, Sherjil Ozair, Aaron C. Courville, and Yoshua Bengio. Generative adversarial nets. In *Advances in Neural Information Processing Systems*, volume 27, pp. 2672–2680, 2014.

Tiankai Hang, Shuyang Gu, Chen Li, Jianmin Bao, Dong Chen, Han Hu, Xin Geng, and Baining Guo. Efficient diffusion training via min-snr weighting strategy. In *Proceedings of the IEEE/CVF International Conference on Computer Vision (ICCV)*, pp. 7441–7451, October 2023.

Martin Heusel, Hubert Ramsauer, Thomas Unterthiner, Bernhard Nessler, and Sepp Hochreiter. Gans trained by a two time-scale update rule converge to a local nash equilibrium. *Advances in neural information processing systems*, 30, 2017.

Jonathan Ho and Tim Salimans. Classifier-free diffusion guidance. In *NeurIPS 2021 Workshop on Deep Generative Models and Downstream Applications*, 2021.

Jonathan Ho, Ajay Jain, and Pieter Abbeel. Denoising diffusion probabilistic models. In *Advances in Neural Information Processing Systems*, volume 33, pp. 6840–6851, 2020.

Jonathan Ho, William Chan, Chitwan Saharia, Jay Whang, Ruiqi Gao, Alexey Gritsenko, Diederik P Kingma, Ben Poole, Mohammad Norouzi, David J Fleet, et al. Imagen video: High definition video generation with diffusion models. *arXiv preprint arXiv:2210.02303*, 2022a.

Jonathan Ho, Tim Salimans, Alexey A. Gritsenko, William Chan, Mohammad Norouzi, and David J. Fleet. Video diffusion models. In *Advances in Neural Information Processing Systems*, pp. 8633–8646, 2022b.

Tero Karras, Samuli Laine, and Timo Aila. A style-based generator architecture for generative adversarial networks. In *CVPR*, pp. 4401–4410, 2019.

Tero Karras, Miika Aittala, Timo Aila, and Samuli Laine. Elucidating the design space of diffusion-based generative models. In *Advances in Neural Information Processing Systems*, 2022.

Bahjat Kawar, Gregory Vaksman, and Michael Elad. Snips: Solving noisy inverse problems stochastically. *Advances in Neural Information Processing Systems*, 34:21757–21769, 2021.

Bahjat Kawar, Michael Elad, Stefano Ermon, and Jiaming Song. Denoising diffusion restoration models. *Advances in Neural Information Processing Systems*, 35:23593–23606, 2022.

Diederik P Kingma, Tim Salimans, Ben Poole, and Jonathan Ho. Variational diffusion models. In *Advances in Neural Information Processing Systems*, 2021.

Zhifeng Kong, Wei Ping, Jiaji Huang, Kexin Zhao, and Bryan Catanzaro. Diffwave: A versatile diffusion model for audio synthesis. In *International Conference on Learning Representations*, 2021.

Alex Krizhevsky, Geoffrey Hinton, et al. Learning multiple layers of features from tiny images. 2009.

Lijiang Li, Huixia Li, Xiawu Zheng, Jie Wu, Xuefeng Xiao, Rui Wang, Min Zheng, Xin Pan, Fei Chao, and Rongrong Ji. Autodiffusion: Training-free optimization of time steps and architectures for automated diffusion model acceleration. In *Proceedings of the IEEE/CVF International Conference on Computer Vision*, pp. 7105–7114, 2023.

Tsung-Yi Lin, Michael Maire, Serge Belongie, James Hays, Pietro Perona, Deva Ramanan, Piotr Dollár, and C Lawrence Zitnick. Microsoft coco: Common objects in context. In *ECCV*, pp. 740–755. Springer, 2014.

Enshu Liu, Xuefei Ning, Zinan Lin, Huazhong Yang, and Yu Wang. Oms-dpm: Optimizing the model schedule for diffusion probabilistic models. In *International Conference on Machine Learning*, pp. 21915–21936. PMLR, 2023a.

Enshu Liu, Xuefei Ning, Huazhong Yang, and Yu Wang. A unified sampling framework for solver searching of diffusion probabilistic models. In *The Twelfth International Conference on Learning Representations*, 2023b.

Luping Liu, Yi Ren, Zhijie Lin, and Zhou Zhao. Pseudo numerical methods for diffusion models on manifolds. In *International Conference on Learning Representations*, 2022.

Cheng Lu, Yuhao Zhou, Fan Bao, Jianfei Chen, Chongxuan Li, and Jun Zhu. Dpm-solver: A fast ode solver for diffusion probabilistic model sampling in around 10 steps. In *Advances in Neural Information Processing Systems*, 2022a.

Cheng Lu, Yuhao Zhou, Fan Bao, Jianfei Chen, Chongxuan Li, and Jun Zhu. Dpm-solver++: Fast solver for guided sampling of diffusion probabilistic models. *arXiv preprint arXiv:2211.01095*, 2022b.

Eric Luhman and Troy Luhman. Knowledge distillation in iterative generative models for improved sampling speed. *arXiv preprint arXiv:2101.02388*, 2021.

Weijian Luo, Tianyang Hu, Shifeng Zhang, Jiacheng Sun, Zhenguo Li, and Zhihua Zhang. Diff-instruct: A universal approach for transferring knowledge from pre-trained diffusion models. *Advances in Neural Information Processing Systems*, 36, 2024.

Xinyin Ma, Gongfan Fang, and Xinchao Wang. Deepcache: Accelerating diffusion models for free. In *Proceedings of the IEEE/CVF Conference on Computer Vision and Pattern Recognition*, pp. 15762–15772, 2024.

Chenlin Meng, Yang Song, Jiaming Song, Jiajun Wu, Jun-Yan Zhu, and Stefano Ermon. SDEdit: Image synthesis and editing with stochastic differential equations. In *International Conference on Learning Representations*, 2022.

Dustin Podell, Zion English, Kyle Lacey, Andreas Blattmann, Tim Dockhorn, Jonas Müller, Joe Penna, and Robin Rombach. Sdxl: Improving latent diffusion models for high-resolution image synthesis. In *International Conference on Learning Representations*, 2024.

Herbert E. Robbins. *An Empirical Bayes Approach to Statistics*, pp. 388–394. Springer New York, New York, NY, 1992. ISBN 978-1-4612-0919-5. doi: 10.1007/978-1-4612-0919-5_26. URL https://doi.org/10.1007/978-1-4612-0919-5_26.

Robin Rombach, Andreas Blattmann, Dominik Lorenz, Patrick Esser, and Björn Ommer. High-resolution image synthesis with latent diffusion models. In *Proceedings of the IEEE/CVF Conference on Computer Vision and Pattern Recognition (CVPR)*, pp. 10684–10695, June 2022.

Nataniel Ruiz, Yuanzhen Li, Varun Jampani, Yael Pritch, Michael Rubinstein, and Kfir Aberman. Dreambooth: Fine tuning text-to-image diffusion models for subject-driven generation. In *Proceedings of the IEEE/CVF Conference on Computer Vision and Pattern Recognition*, pp. 22500–22510, 2023.

Amirmojtaba Sabour, Sanja Fidler, and Karsten Kreis. Align your steps: Optimizing sampling schedules in diffusion models. *arXiv preprint arXiv:2404.14507*, 2024.

Chitwan Saharia, William Chan, Saurabh Saxena, Lala Li, Jay Whang, Emily L Denton, Kamyar Ghasemipour, Raphael Gontijo Lopes, Burcu Karagol Ayan, Tim Salimans, et al. Photorealistic text-to-image diffusion models with deep language understanding. In *Advances in Neural Information Processing Systems*, pp. 36479–36494, 2022.

Tim Salimans and Jonathan Ho. Progressive distillation for fast sampling of diffusion models. In *International Conference on Learning Representations*, 2022.

Axel Sauer, Dominik Lorenz, Andreas Blattmann, and Robin Rombach. Adversarial diffusion distillation. *arXiv preprint arXiv:2311.17042*, 2023.

Chenyang Si, Ziqi Huang, Yuming Jiang, and Ziwei Liu. Freeu: Free lunch in diffusion u-net. In *Proceedings of the IEEE/CVF Conference on Computer Vision and Pattern Recognition*, pp. 4733–4743, 2024.

Jascha Sohl-Dickstein, Eric Weiss, Niru Maheswaranathan, and Surya Ganguli. Deep unsupervised learning using nonequilibrium thermodynamics. In *International Conference on Machine Learning*, pp. 2256–2265. PMLR, 2015.

Jiaming Song, Chenlin Meng, and Stefano Ermon. Denoising diffusion implicit models. In *International Conference on Learning Representations*, 2021a.

Jiaming Song, Arash Vahdat, Morteza Mardani, and Jan Kautz. Pseudoinverse-guided diffusion models for inverse problems. In *International Conference on Learning Representations*, 2023a.

Yang Song, Jascha Sohl-Dickstein, Diederik P. Kingma, Abhishek Kumar, Stefano Ermon, and Ben Poole. Score-based generative modeling through stochastic differential equations. In *International Conference on Learning Representations*, 2021b.

Yang Song, Liyue Shen, Lei Xing, and Stefano Ermon. Solving inverse problems in medical imaging with score-based generative models. In *International Conference on Learning Representations*, 2022.

Yang Song, Prafulla Dhariwal, Mark Chen, and Ilya Sutskever. Consistency models. In *International Conference on Machine learning*, pp. 32211–32252, 2023b.

Daniel Watson, William Chan, Jonathan Ho, and Mohammad Norouzi. Learning fast samplers for diffusion models by differentiating through sample quality. In *International Conference on Learning Representations*, 2022.

Mengfei Xia, Yujun Shen, Changsong Lei, Yu Zhou, Deli Zhao, Ran Yi, Wenping Wang, and Yong-Jin Liu. Towards more accurate diffusion model acceleration with a timestep tuner. In *Proceedings of the IEEE/CVF Conference on Computer Vision and Pattern Recognition (CVPR)*, pp. 5736–5745, June 2024.

Shuchen Xue, Mingyang Yi, Weijian Luo, Shifeng Zhang, Jiacheng Sun, Zhenguo Li, and Zhi-Ming Ma. Sa-solver: Stochastic adams solver for fast sampling of diffusion models. *Advances in Neural Information Processing Systems*, 36, 2024.

Fisher Yu, Ari Seff, Yinda Zhang, Shuran Song, Thomas Funkhouser, and Jianxiong Xiao. Lsun: Construction of a large-scale image dataset using deep learning with humans in the loop. *arXiv preprint arXiv:1506.03365*, 2015.

Qinsheng Zhang and Yongxin Chen. Fast sampling of diffusion models with exponential integrator. In *The Eleventh International Conference on Learning Representations*, 2022.

Wenliang Zhao, Lujia Bai, Yongming Rao, Jie Zhou, and Jiwen Lu. Unipc: A unified predictor-corrector framework for fast sampling of diffusion models. In *Advances in Neural Information Processing Systems*, pp. 49842–49869, 2023.

Kaiwen Zheng, Cheng Lu, Jianfei Chen, and Jun Zhu. Dpm-solver-v3: Improved diffusion ode solver with empirical model statistics. *Advances in Neural Information Processing Systems*, 36: 55502–55542, 2023.

Zhenyu Zhou, Defang Chen, Can Wang, and Chun Chen. Fast ode-based sampling for diffusion models in around 5 steps. In *Proceedings of the IEEE/CVF Conference on Computer Vision and Pattern Recognition (CVPR)*, pp. 7777–7786, June 2024.

A FID Results for DLMS and Handcrafted Solvers.

Table 4: Comparison of FID↓ scores between DLMS and handcrafted solvers.

Dataset	Solver	NFE						
		4	5	6	7	8	9	10
CIFAR10	DEIS	25.66	14.39	9.40	6.94	5.55	4.68	4.09
	DPM-Solver++	46.52	24.97	11.99	6.74	4.54	3.42	3.00
	UniPC	45.20	23.98	11.14	5.83	3.99	3.21	2.89
	DLMS	**4.52**	**3.23**	**2.81**	**2.53**	**2.43**	**2.37**	**2.24**
FFHQ	DEIS	28.31	17.36	12.25	9.37	7.59	6.39	5.56
	DPM-Solver++	45.95	22.51	13.74	8.44	6.04	4.77	4.12
	UniPC	44.78	21.40	12.85	7.44	5.50	4.47	**3.84**
	DLMS	**9.63**	**6.85**	**5.82**	**5.16**	**4.81**	**4.23**	4.12
ImageNet-64	DEIS	23.53	14.75	12.57	8.20	6.84	5.97	5.34
	DPM-Solver++	56.63	25.49	15.06	10.14	7.84	6.48	5.67
	UniPC	55.63	24.36	14.30	9.57	7.52	6.34	5.53
	DLMS	**10.07**	**7.16**	**7.08**	**6.31**	**5.93**	**4.57**	**4.30**
LSUN-Bedroom	DEIS	12.89	6.83	5.35	4.78	4.43	4.25	4.05
	DPM-Solver++	48.49	18.44	8.39	5.18	4.12	3.77	3.60
	UniPC	39.66	13.76	6.46	4.52	3.96	3.72	3.56
	DLMS	**8.20**	**5.44**	**4.44**	**3.99**	**3.89**	**3.70**	**3.50**
ImageNet	DPM-Solver++	26.30	17.08	13.06	11.08	9.95	9.25	8.72
	UniPC	24.99	15.71	11.95	10.24	9.36	**8.82**	8.45
	DLMS	**19.74**	**13.83**	**10.90**	**9.66**	**9.07**	8.89	**8.22**
MS-COCO	DEIS	-	**15.16**	13.95	13.61	13.58	13.46	13.38
	DPM-Solver++	-	17.40	15.78	15.08	14.77	14.43	14.18
	UniPC	-	17.33	15.70	15.06	14.74	14.44	14.28
	DLMS	-	15.69	**13.54**	**13.20**	**13.07**	**12.69**	**11.72**

B More Qualitative Results

(a) DEIS, FID=25.66 (b) DLMS, FID=4.52

Figure 5: Uncurated samples on CIFAR10 32×32 with 4 NFE.

(a) DEIS, FID=28.31

(b) DLMS, FID=9.63

Figure 6: Uncurated samples on FFHQ 64×64 with 4 NFE.

(a) DEIS, FID=14.75

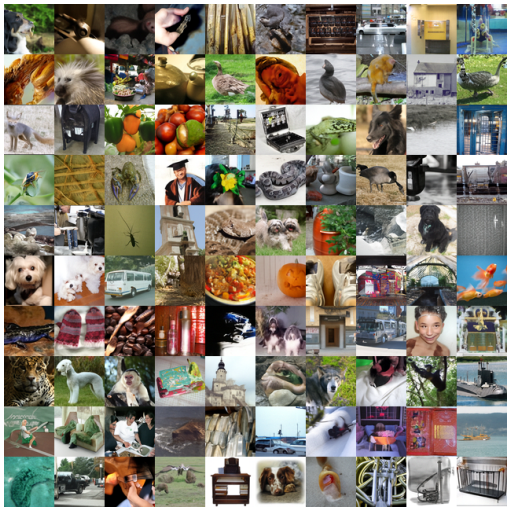

(b) DLMS, FID=7.16

Figure 7: Uncurated samples on ImageNet-64 64×64 with 5 NFE.

(a) DEIS, FID=12.89 (b) DLMS, FID=8.20

Figure 8: Uncurated samples on LSUN-Bedroom 256×256 with 4 NFE.

Table 5: Additional samples of Stable-Diffusion (Rombach et al., 2022) with a classifier-free guidance scale 7.5, using only 10 NFE and selected text prompts.

Text Prompts	DPM-Solver++ (FID=14.18)	DEIS (FID=13.38)	DLMS (FID=11.72)
"a sandwich on wheat bread sits on a plate"			
"three big elephants walking across a wide river"			
"Air force jet in a take off position above the tree line."			
"An empty bench next to a potted tree up against a brick wall."			
"A star hangs upon a canopied bed in a bedroom."